Copyright © 2009 Tech Science Press CMES, vol.40, no.1, pp.83-103, 2009

Study of the Underfill Effect on the Thermal Fatigue Life of WLCSP-Experiments and Finite Element Simulations

Shaw-Jyh Shin[1], Chen-Hung Huang[2] and Y.C. Shiah[3]

Abstract: Owing to the CTE (Coefficient of Thermal Expansion) mismatch among solder joints, IC (Integrated Circuit) chip, and PCB (Printed Circuit Board), electronic packages shall experience fatigue failure after going though a period of thermal cycling. As a major means to enhance the reliability of the solder joints, underfill is often dispensed to fill the gap between the die and the substrate. This study aims at investigating how the underfill may affect the thermal fatigue life of WLCSP (Wafer Level Chip Scale Package) by means of FEA (finite element analysis). In this study, the thermal fatigue life of the WLCSP was simulated using full-model. For comparison with the FEA simulations, experiments were also conducted for a few WLCSP with/without underfill.

Keywords: Thermal fatigue life of WLCSP, underfill, finite element analysis.

1 Introduction

Recently, 3C (computer, communication, and consumer electronics) products on the market tend to be portable and light-weight, yet has increased functionality to cater for consumers' fashion. These demands have driven the IC packaging move from Pin Through Hole to Surface Mount Technology. Instead of assembling the package of each individual unit after wafer dicing, recent technology has progressed to Wafer Level Chip Scale Packaging (WLCSP), producing packages practically of the same size as the die. Indeed, the WLCSP technology has laid the foundation for true integration of wafer fab, packaging, test, and burn-in at wafer level, for the ultimate streamlining of the manufacturing process.

The CTE (Coefficient of Thermal Expansion) is a temperature-dependent material property of metals and has been analyzed by Chiang, Chou, Wu, Huang and Yew

[1] Dept. of Communications Eng., Feng Chia University, R.O.C.
[2] Dept. of Aerospace and Systems Eng., Feng Chia University, R.O.C.
[3] Corresponding Author. Dept. of Aerospace and Systems Eng., Feng Chia University, R.O.C., Email: ycshiah@fcu.edu.tw

(2008), its mismatch among the solder joint, IC chip, and PCB is the main cause of the package's failure, and significant thermal stresses shall occur on the joined interfaces owing to the CTE . The low melting point of solder balls makes its creep strain behavior more likely to cause the fatigue failure than other packaging materials do. Given this, the signal transmission of electronic packaging will become less effective, even failing at times. This problem is even more serious for WLCSP, whose solder balls are comparably small. Due to this, the reliability analysis of solder joints of WLCSP subjected to thermal cycling has been an important research topic in the electronic packaging community. As schematically shown in Fig. 1, a major means to enhance the reliability of solder joints is to fill the gap between the die and the substrate with underfill; however this process will increase the manufacturing cost. Therefore, a concern may arise regarding how effective the underfill may enhance the reliability when one is facing the cost tradeoff.

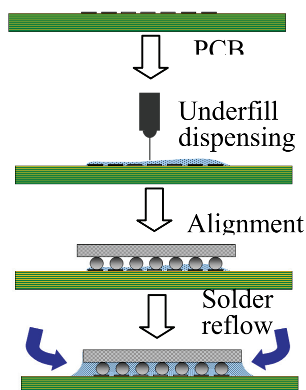

Figure 1: No-flow underfill of WLCSP

The conventional way for assessing a package's thermal fatigue life often resorts to thermal cycling experiments that are not only time-consuming but also costly. Although various accelerated tests have been widely adopted to expedite the assessment, the test process still requires a long period of time in general. The goal of this study is to apply a viscoplastic constitutive model based on the approach of Anand (1985) to investigate the effect of underfill (Fig. 1) on the reliability of solder balls of a WLCSP. The WLCSP, manufactured by a renowned company in the electronic industry, has unsymmetrical layout of ball grid array (BGA) as shown in Fig. 2.

In principal, the unsymmetrical layout shall require full FEA modeling that takes a considerable amount of elements. To improve the efficiency of the full mod-

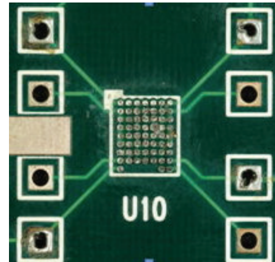

Figure 2: Layout of the WLCSP ball grid array

eling, we propose a sub-modeling technique that performs global analysis with a coarsely meshing scheme, subsequently following with local analysis employing refined meshes around solder balls. This differs from the solution procedure of the commonly used Global-Local FEA modeling. Since the BGA layout of the present WLCSP is nearly symmetrical, we also applies the slice model and the quarter model to analyze its thermal fatigue life as comparison of the analysis using the full modeling.

So far, to the authors' knowledge, pertinent studies for investigating the underfill effect of WLCSP still remain comparably scarce in the open literature. Sun, Hochstenbach, Van Driel and Zhang (2008) experimentally analyzed the brittle fracture of intermetallic compound under high-speed pull condition. Tsai, Lai, Yeh and Chen (2008) applied the Taguchi optimization method to obtain the optimal design in enhancing board-level drop reliability of a WLCSP. For Chip Scale packages, Lee, Nguyen and Selvaduray (2000) gave a review of fourteen solder joint fatigue models with an emphasis on summarizing the features and applications of each fatigue model. In recent years, a number of solder fatigue life models have been developed to predict the thermal fatigue life of solder joint [e.g. Manson (1996); John, Wang, John and Wataru (1998); Amagai (1999); Cheng, Yu and Chen (2005)]. These models, being categorized into stress-based, plastic-strain-based, creep-strain-based, energy-based, and damage-based methods, utilize non-elastic strain range and viscoplastic strain energy density to estimate the fatigue life of solder joints. For the present work, an integrated constitutive model with viscoelastic, plastic, and creep behaviors is adopted for the solder joints to ensure the accuracy. The analysis employs Darveaux's approach [Darveaux (1995)], based on viscoplastic strain energy density, to predict the thermal fatigue life of solder balls. Additionally, to take into account the effects of cyclic frequency and temperature profile, the Engelmaier fatigue life model [Engelmaier (1983)], a modified Coffin-Manson formula based on shear strain increment, is also adopted for computation

of the thermal fatigue life. Sequentially, the reliability of the package is evaluated by a two-parameter Weibull failure distribution.

To verify our predictions, WLCSP samples with daisy chain connection were experimented with a programmable temperature chamber, providing cyclic temperature variation of $0^0C \sim 100^0C$ until failure occurred. To monitor the failure in real-time, the electric resistance of the samples that were connected to Agilent 34970A outside the temperature chamber was recorded by BenchLink DataLogger. The experiment was conducted for the both WLCSP types as comparison- one with underfill and the other without underfill.

2 Theoretical fundamentals

The fundamentals of the thermal fatigue analysis in this study include Two Parameter Weibull Distribution [Lai, Wang, Tsai and Jen (2007)], Anand's model [Anand (1985)], and a few methodologies for predicting the thermal fatigue life of solder balls. Before our Finite Element analysis for the WLCSP is presented, the fundamentals are reviewed as a start.

The Weibull distribution [Weibull (1951)], a continuous probability distribution named after Waloddi Weibull, is often used to describe the statistical distribution of fracture in engineering reliability assessment. The Weibull distribution takes the form,

$$f(T) = \frac{\beta}{\eta}\left(\frac{T-\gamma}{\eta}\right)^{\beta-1} e^{-\left(\frac{T-\gamma}{\eta}\right)^{\beta}} = \lambda\left(T\right)R\left(T\right), \tag{1}$$

where T is the cyclic number, β is the shape parameter (or Weibull slope), γ is position function, and η is scale parameter (or characteristic life). In Equation (1), $\lambda\left(T\right) = \frac{\beta}{\eta}\left(\frac{T-\gamma}{\eta}\right)^{\beta-1}$ is defined as the Weibull failure function and $R\left(T\right) = e^{-\left(\frac{T-\gamma}{\eta}\right)^{\beta}}$ is the Weibull reliability function. When γ=0, Equation (1) becomes

$$f_2\left(T\right) = \frac{\beta}{\eta}\left(\frac{T}{\eta}\right)^{\beta-1} e^{-\left(\frac{T}{\eta}\right)^{\beta}} = \lambda_2\left(T\right)R_2\left(T\right), \tag{2}$$

which is referred to as the Two Parameter Weibull Distribution. More details regarding the Two Parameter Weibull Distribution can be referred to Prabhakar Murthy, Bulmer and Eccleston (2004).

The stress or strain-rate of viscoplastic materials exhibits a time-dependent behavior. For most materials, the typical plastic theory is accurate enough to describe their material behaviors; however, some metals exhibit both creep and plastic behaviors, especially under high temperature. The solder balls of the WLCSP, made

of 63Sn/37Pb alloy, has the melting point 456°K. For the thermal cycles with peak temperature at 100°C, the solder balls will undergo significant creep. According to Knecht and Fox (1991), the total strain rate includes the elastic strain rate $\dot{\gamma}_e$, the plastic strain rate $\dot{\gamma}_{pl}$, and the creep strain rate $\dot{\gamma}_{cr}$, i.e.

$$\dot{\gamma}_{tot} = \dot{\gamma}_e + \dot{\gamma}_{pl} + \dot{\gamma}_{cr}, \tag{3}$$

which leads to the total stress

$$\dot{\tau}_{tot} = \left[\frac{1}{G} + A\frac{m}{\tau_p^m}\tau^{m-1}\right]\dot{\tau} + B\tau^n. \tag{4}$$

In Equation (4), A, B, m are material constants. According to Anand's model, the viscoplastic behavior should be taken into consideration when the operational temperature is greater than half of the melting point of the material. This kind of behavior appears to be similar to the creep behavior, but it is a bit more complicated than that. For the approach, Anand used the constitutive law for creep and an anti-deformation factor s to formulate the rate of equivalent plastic strain $d\varepsilon_{eq}/dt$ as

$$\frac{d\varepsilon_{eq}}{dt} = A\left[\sinh\left(\zeta\frac{\sigma}{s}\right)\right]^{1/m} e^{\left(-\frac{Q}{KT}\right)}, \tag{5}$$

where Q is the activation energy, m is the strain-rate sensitivity, K is the Boltzmann constant, ζ is multiplier of stress, A is the pre-exponential factor, s is the anti-deformation factor, T is the absolute temperature, and σ is effective Cauchy stress. The time derivative of the anti-deformation factor in Eq. (5) is defined by

$$\dot{s} = h_0\left[(|B|)^a \cdot (B/|B|)\right](d\varepsilon_{eq}/dt), \tag{6}$$

$$B = 1 - s/s^*, \tag{7}$$

$$s^* = \hat{s}\left[\varepsilon_{eq}e^{(Q/KT)}/A\right]^n, \tag{8}$$

where a is the sensitivity of strain rate, h_0 is the material's hardening constant, s^* is the initial value of deformation resistance, $\hat{s}$ is the coefficient for saturated s^*, and n is the strain rate sensitivity of saturation. All these constants for the Anand's model are tabulated in Tab. 1.

To predict the fatigue life of the solder joint, the present study adopts Darveaux's strain-energy based method [Darveaux (1995)], using visco-plastic strain energy density for determination of the fatigue failure of solder balls subjected to thermal cycling. However, several studies revealed that the viscoplastic strain energy was sensitive to mesh density of FEA model. The strategy to make the strain-energy

based approach more robust is to apply the volumetric averaging technique, reducing the sensitivity of the viscoplastic strain energy density to mesh density. Further, Darveaux suggested picking the viscoplastic strain energy density after three complete thermal cycles to obtain stabilized values and reduce the effect of stress singularity.

Table 1: Constants used for the Anand's model

Parameter	Value	Unit	Definition
S^*	1800	Psi	initial value of deformation resistance
Q/k	9400	1/K	activation energy / Boltzmann's
A	4.0E6	1/sec	pre-exponential factor
ζ	1.5	*	multiplier of stress
m	0.303	*	strain rate sensitivity
h_0	2.0E5	Psi	hardening constant
$\hat{s}$	2.0E3	Psi	coefficient for deformation resistance saturation value
n	0.07	*	strain rate sensitivity of saturation
a	1.3	*	strain rate sensitivity of hardening

Note: * is dimensionless

The average viscoplastic strain-energy density accumulated per cycle is expressed as

$$\Delta W_{ave} = \frac{\sum \Delta W \cdot V}{\sum V} \tag{9}$$

where ΔW represents the viscoplastic strain energy density accumulated per cycle for each interface element; V is the volume for each interface element of solder joint. Still, the approach is strongly dependable on element volume. Thus, several sets of empirical constants were recommended by Darveaux (1995) to calculate the viscoplastic strain density of the interface element with different thicknesses. Once the strain-energy density is obtained, the number of cycles for crack initiation can thus be calculated using

$$N_0 = K_1 \cdot \Delta W_{ave}^{K_2}, \tag{10}$$

and the crack growth rate per thermal cycle is obtained via

$$da/dN = K_3 \cdot \Delta W_{ave}^{K_4}, \tag{11}$$

where crack growth constants $K_1 \sim K_4$ given by Darveaux (1995); a is the crack length (i.e. the diameter of the solder joint at interface). Consequently, the characteristic fatigue life of solder joint (i.e. number of cycles to yield 63.2% of the population failed), denoted by α, can be acquired through

$$\alpha = N_0 + \frac{a}{da/dN} \tag{12}$$

To take the effects of cyclic frequency and temperature range into account, the Engelmaier fatigue life model [Engelmaier (1983)], a modified Coffin-Manson formula based on shear strain increment is adopted to compute the fatigue life of solder joint. The total number of cycles to failure, N_f, is given by

$$N_f = 0.5\left(\Delta\gamma/2\varepsilon_f'\right)^{\frac{1}{c}}, \tag{13}$$

where $\Delta\gamma$ is the shear strain increment (range), and ε_f' is the fatigue ductility coefficient. In Eq. (9), the value of $2\varepsilon_f'$ is approximately 0.65 for 63Sn/37Pb alloy; C, referring to the fatigue ductility exponent, is given (for $1 \le f \le 1{,}000$ cycles/day) by

$$C = -0.442 - 6\times10^{-4}T_m + 1.74\times10^{-2}\ln(1+f), \tag{14}$$

where T_m is the average temperature in Celsius, and f is the cyclic frequency.

According to von Mises yield criterion, the relationship between shear strain and von Mises strain can be expressed [Weibull (1951); Murthy, Bulmer and Eccleston (2004)] as

$$\gamma = \sqrt{3}\varepsilon, \tag{15}$$

where γ is the shear strain; ε_{von} is the von Mises strain defined as

$$\varepsilon_{von} = \frac{\sqrt{2}}{3}\left[(\varepsilon_x-\varepsilon_y)^2+(\varepsilon_y-\varepsilon_z)^2+(\varepsilon_x-\varepsilon_z)^2+\frac{3}{2}\left(\gamma_{xy}^2+\gamma_{yz}^2+\gamma_{zx}^2\right)\right]^{\frac{1}{2}}. \tag{16}$$

From Eq. (13), the equivalent shear strain increment can be expressed as

$$\Delta\gamma = \sqrt{3}\Delta\varepsilon_{von} \tag{17}$$

where $\Delta\varepsilon_{von}$ refers to the von Mises strain increment given by the difference between the largest and the smallest von Mises strain in each thermal cycle. By substituting Eq. (15) into Eq. (11), the total number of cycles to failure can be rewritten as follows:

$$N_f = \frac{1}{2}\left(\frac{\sqrt{3}\Delta\varepsilon_{von}}{2\varepsilon_f'}\right)^{\frac{1}{c}}. \tag{18}$$

As a result, with $\Delta\varepsilon_{von}$ obtained through finite element analysis, the fatigue life of the solder joint (i.e. the average number of cycles to failure) can be estimated by Eq. (16). In what follows, description of our FEA simulation for real WLCSP specimens provided by the industry will be addressed next. Additionally, for verifying the fidelity of our simulation, experiment to test the fatigue life of the WLCSP specimens was conducted. The aforementioned method is employed to predict the thermal fatigue life of the solder joint.

For assessment of the overall reliability, Weibull-distribution, working ideally for fatigue fracture, is the most commonly used statistical distribution to describe the wear out and fatigue failures in solder joints. Further, the reliability of the package, R, can be evaluated by a two-parameter Weibull distribution as follows :

$$R = e^{-(N/N_\alpha)^\beta}, \tag{19}$$

where N is the number of thermal cycles for R. The parameters N_α and β ($2.6 \leq \beta \leq 4.0$) represent the characteristic life of the package and the slop of Weibull distribution, respectively. Using Equation (17), the number of cycles for the package failure can be readily calculated from the characteristic fatigue life of the solder joints along with a given β.

3 Experiments & Computer Simulations

To reduce the experimental period, more rigorous loading conditions than the actual, including the cyclic frequency and the range of temperature variations, are usually designed to accelerate the package's failure for rapidly predicting the fatigue life of solder balls. The fatigue life under actual field-use conditions can be obtained through the use of an acceleration factor AF defined as follows [Pang and Chong (2001)]:

$$AF = N_{f(F)}/N_{f(L)} = \left[\frac{\Delta T_L}{\Delta T_F}\right]\left[\frac{f_F}{f_L}\right]^{\frac{1}{m}} e^{\left[\frac{0.123}{K}\left(\frac{1}{(T\max)_F} - \frac{1}{(T\max)_L}\right)\right]}, \tag{20}$$

where the subscripts L and F refer to the laboratory conditions and field-use conditions respectively, $N_{f(F)}$ and $N_{f(L)}$ represent the fatigue life of package under field-use and laboratory conditions respectively, ΔT is the difference between the maximum and minimum temperature in each thermal cycle, K is the Boltzamann constant, f is the cyclic frequency within the range from 1 to 1000 cycles/day, values of n and m are equal to 1.9 and 3 respectively, and $T_{\max}$ is the peak temperature. Owing to the very limited power of the cooling compressor of our programmable temperature chamber (Fig. 3 (a)), cooling the chamber temperature from 100°C to 0°C may take up to 40 minutes for each thermal cycle.

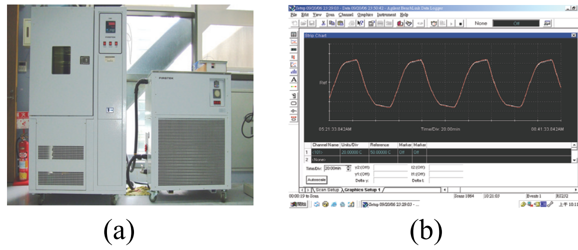

(a) (b)

Figure 3: (a) Programmable temperature chamber; (b) temperature profile

The long duration of this cooling process will significantly delay the failure of solder balls. For this, an extra circulating liquid cooling system, filled with industrial alcohol, is connected to the programmable temperature chamber to speed up the cooling process. Further, the cyclic temperature profile is divided into four stages: (1) temperature rising up to 100°C, (2) constant temperature sustained at 100°C, and (3) temperature dropping to 0°C, and (4) constant temperature sustained at 0°C, each of which lasts approximately 14 minutes. With the added cooling system, the programmable temperature chamber is boosted to have the temperature profile for the four temperature stages as shown in Fig. 3(b).

Shown in Fig. 4 is the front view of three different groups of WLCSP mounted on a printed circuit board. Each group of the same packaging type contains eight WLCSP specimens to be tested.

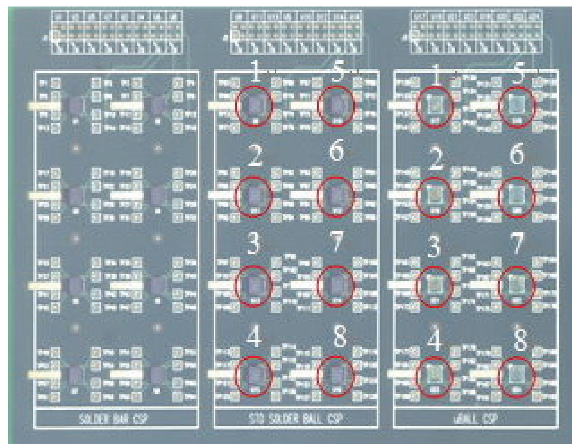

Figure 4: WLCSP specimens for the thermal fatigue test

The packaging types of the three grouped packages from left to right are characterized as the Solder Bar, the STD Solder Ball, and the uBall with underfill, respectively. Figure 5(a) shows the appearance of each WLCSP; Figure 5(b) depicts the daisy chain connection of each unit. Figures 5(a) and 5(b) also depict the I/O connections (two input and two output channels) of each specimen connected to the data acquisition instrument. As shown in the figures, there are 8 through-hole connections, through which the signals of resistance and temperature of the chip are transmitted to Agilent 34970A.

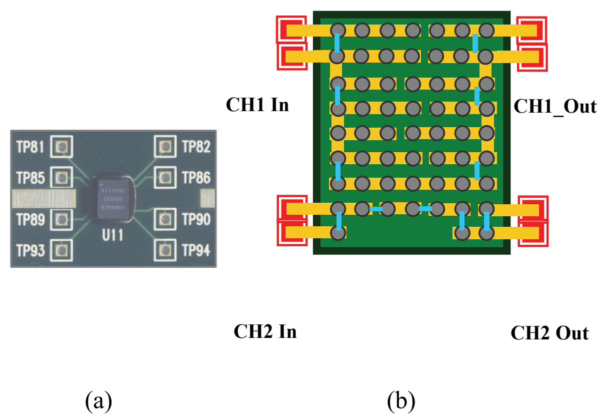

Figure 5: (a) WLCSP sample; (b) daisy chain connection

For investigating the underfill effect, only the STD Solder Ball and the uBall groups were connected to Agilent 34970A for recording the variation of the units' electric resistance by DataLogger (see Fig. 6). With the increase of thermal cycles, the viscoplastic strain energy of the solder balls would accumulate until fatigue fracture occurred. As shown in Fig. 7, the electric resistance of a unit would fluctuate drastically when the fatigue was triggered. When the failure occurred, the electrical resistance would go to infinity and, thus, the fatigue lives of packages were identified. The data acquisition instrument, Agilent 34970A, measured the data every 20 seconds and the duration of a complete thermal cycle lasted 56.2 minutes. Therefore, the number of thermal cycles applied to the test specimen could be obtained from the total number of data sets. Figure 8 shows the cross sectional view of a fractured solder ball in the uBall group after the thermal fatigue occurred.

From the recorded history of the electric resistance of all WLCSP units, the numbers of undergone thermal cycles before thermal fatigue had occurred were deter-

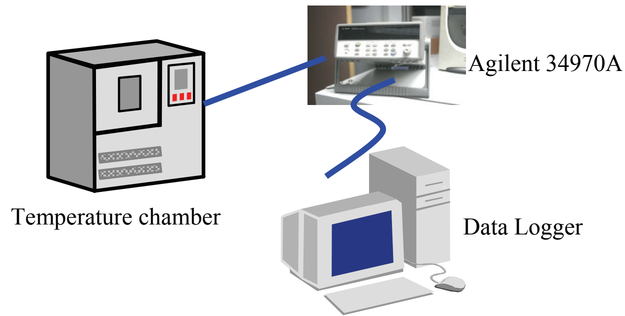

Figure 6: Experimental setup for the thermal fatigue test

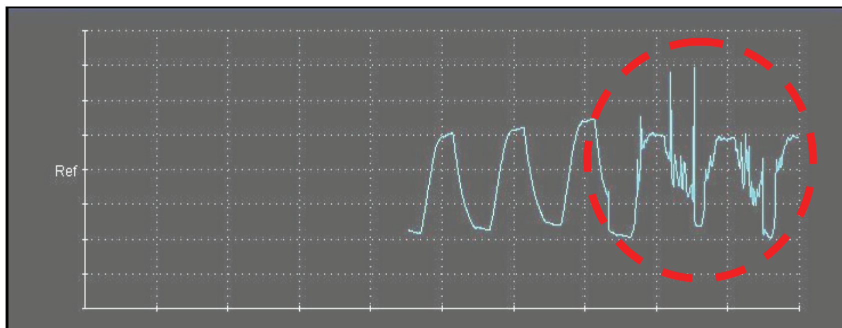

Figure 7: Fluctuation of electric resistance

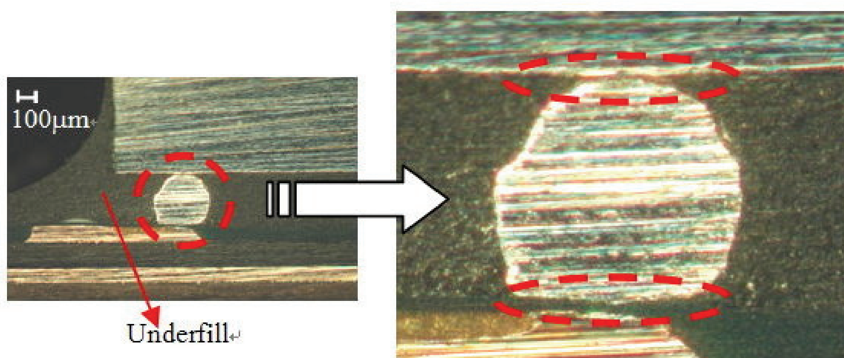

Figure 8: Thermal fatigue fracture of a solder ball

mined for all units. Under the same experimental environment, this experiment was conducted continuously twice for two identical PCBs, taking about six months to complete. The average thermal fatigue lives of the packages were found to be 1315 (cycles) and 2181 (cycles) for the STD group and the uBall group, respectively. From the experimental result, it was found that the use of underfill might increase the WLCSP's thermal fatigue life by 65.9% or so.

With each thermal cycle taking 56.2 minutes, the complete thermal fatigue experiment took about three months for the uBall group of WLCSP units to fail. In practice, the industry sometimes uses a costly temperature chamber giving a more rigorous temperature profile between -40°C to 100°C to expedite the failure. However, this experimental process still requires 1.5∼2 months at least. To effectively evaluate the reliability of the packages, we also used ANSYS, based upon the Finite Element method, to simulate the experiment. As shown in Fig. 5(b), the layout of solder balls and copper layers are fully unsymmetrical and, thus, full-mesh modeling is principally required. Figure 9 shows the full-mesh model built for the STD packages.

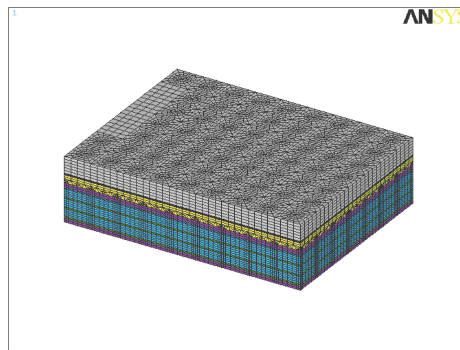

Figure 9: Full-mesh modeling of the WLCSP

All material properties for the ANSYS analysis, provided by the industry, are listed in Tabs. 2 and 3. As noted, the Poisson's ratio and the coefficients of thermal expansion (CTE) of FR-4 substrate are essentially orthotropic. Also, the Young's moduli of FR-4, solder balls, and underfill are all temperature dependent. Perceiving the fact that silicon chip has relatively large Young's Modulus and sustains little or no plastic deformation before fracture, we used linearly elastic elements to analyze it.

For the simulation, element type VISCO107, defined by eight nodes as a three dimensional plastic solid element, was employed to model the solder joints. The use of VISCO107 enables us to acquire the viscoplastic strain-energy density directly

Table 2: Material properties of WLCSP components

Component	Young's Modulus (Mpsi)	Poisson's Ratio	CTE (ppm/°)
Silicon die	23.6	0.278	5.88
Cu layer	17.0681	0.33	17.7
FR-4	4.05-5.39*10^{-3}*T (In-plane) 17.7-2.35*10^{-3}*T (Out-of-plane)	0.39 0.11	16.0 (In-plane) 84.0 (Out-of-plane)
Solder balls (63Sn37Pb)	11.0-2.2*10E-2*T	0.30	24
Underfill	1.206-1.408*10E-3*T	0.35	33
Solder resist	0.6	0.40	30

Note: T is the absolute temperature in Kelvin

through the solution output of elements.

Table 3: Shear moduli of FR-4

	233°K	303°K	373°K	423°K
G_{YZ}(Mpsi) (Out-of-plane)	0.5512	0.4770	0.4028	0.3497
G_{XZ}(Mpsi) (Out-of-plane)	0.5512	0.4770	0.4028	0.3497
G_{XY}(Mpsi) (In-plane)	1.2586	1.0087	0.9187	0.7973

For modeling the underfill, SOLID92 elements were used that might account for creep, plasticity, and large deflection behavior. The PCB consists of multi-layers, each of which has thickness drastically varying from one to another. If adopting the usual 3D elements to model all layers, the modeling of thin layers shall lead to an enormous amount of elements to sustain reasonable aspect ratios of elements. In general, this difficulty may be eased by replacing the stack of layers by a single structure with equivalent mechanical properties. Such equivalence may, of course, greatly reduce the amount of modeling elements, but it will also sacrifice analysis accuracy to a certain degree. For the present simulation, element type SOLID46 is employed, especially designed for modeling thin layers. The rest of other components use SOLID45 elements for the modeling.

The comprehensive full-mesh model started with modeling a solder ball by means of volume revolution and extrusion. Having built the model of a solder ball, the comprehensive full-mesh model was established through object duplication/mirror

and, thereafter, completed by detailed partial refinement. Due to the drastic CTE mismatch between solder balls and solder pads, thermal fatigue fracture is usually initiated somewhere in a solder ball close to the interface. For this, a much refined sub-model is employed to represent the solder ball and its vicinity to yield accurate result. Figure 10 shows the STD sub-model, consisting of 8640 elements with a total of 9982 nodes.

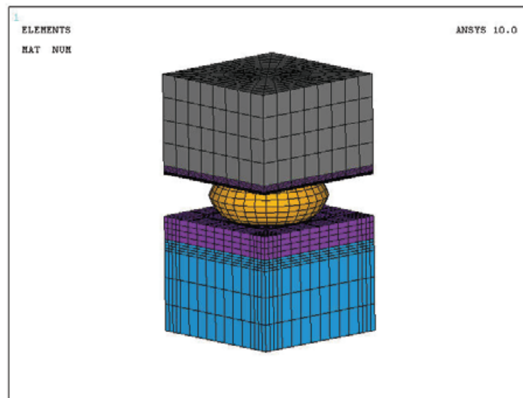

Figure 10: Sub-modeling for the STD solder joints

Mesh size of the sub-model is gradually increased in the radial outward directions from the center of solder balls. The global finite element model contains 133072 elements and 214663 elements for the STD WLCSP and the uBall WLCSP, respectively. The use of sub-model might effectively cut down the computational time to perform iterative computation for the full FEA model with a large number of elements. Our analysis showed that mesh density played a key role in the accuracy of simulation result. Obviously, although globally refining the full model may help increase the accuracy, it will also trade off the computational efficiency at the same time. For improving the accuracy yet with efficiency, we employed a sub-modeling technique discussed as follows.

The technique of sub-modeling is also named as the cut-boundary displacement method or the specified boundary displacement method. In this study, the deformation for the global finite element model was collected after performing iterative computation of four thermal cycles and, subsequently, the recorded data were used to specify the boundary conditions of the sub-model. According to St. Venant's principle, statically equivalent applied loads shall yield the same stress field within regions sufficiently far away from the place where loads are applied. In other words,

the stress field only varies in the loading vicinity for statically equivalent loading systems. Accordingly, the sub-model should still yield accurate results as long as the boundary of the sub-model is sufficiently far away from areas of stress concentration. The main advantage of the sub-modeling is to analyze the complicated problem without starting the simulation from a fine global model. For our simulation, a coarse-mesh model suitable for fast computation was firstly employed to compute preliminary results; sequentially, a sub-model with fine meshes was used to refine the results afterwards. Our numerical experiments showed that the sub-modeling would satisfactorily yield accurate results as compared with those obtained from a global fine model.

To faithfully simulate the temperature profile delivered inherently by the programmable temperature chamber used for the experiment, a complete thermal cycle is divided into 14 identical time steps. The duration of a complete cycle lasts 56.2 minutes with corresponding temperatures specified at each time step. Given the initial temperature (set at 25°C) and the thermal cycling loading, ANSYS, being programmed with APDL (ANSYS Parametric Design Language), would calculate the strain value corresponding to each temperature stage. The same solution procedure was thereafter repeated at each time step except that the strain value obtained from the previous time step served as the initial state (condition) for calculation of the current strain value. Shown in Fig. 11 is the displacement plot for the uBall solder-balls at the 32th time step when it was 100°C. This revealed that the maximum displacement occurred at the lower right corner, and so was the STD unit. Also, this phenomenon could be seen from the distribution of their viscoplastic strain energy, plotted in Fig. 12. Figure 13 shows the computed warping of the package, much exaggerated for better view, at the 32th time step.

After the iterative computations for four thermal cycles were completed, the solder ball with the largest strain energy density was firstly spotted (Fig. 12) and, subsequently, its average viscoplastic strain energy density of the solder-ball was calculated using Equation (7) for its fatigue life. Figures 14(a) and 14(b) show the variations of the total equivalent strain of the solder ball for the STD and uBall WLCSP, respectively.

From the figures, it is apparent to see that the accumulated strain increases as the process goes through each plastic stage. Also, by the comparison between the two cases, one may easily recognize that the total strain of the uBall solder-ball is much smaller than that of the STD package. This explains why the solder-balls with underfill have longer thermal fatigue life. Also, this can be seen from the stress-strain relation of the solder-ball as illustrated in Figs. 15(a) and 15(b) for the STD and uBall WLCSP, respectively. When the temperature rises, stress increases as the strain increases before reaching the yield point of the solder joint. After reaching

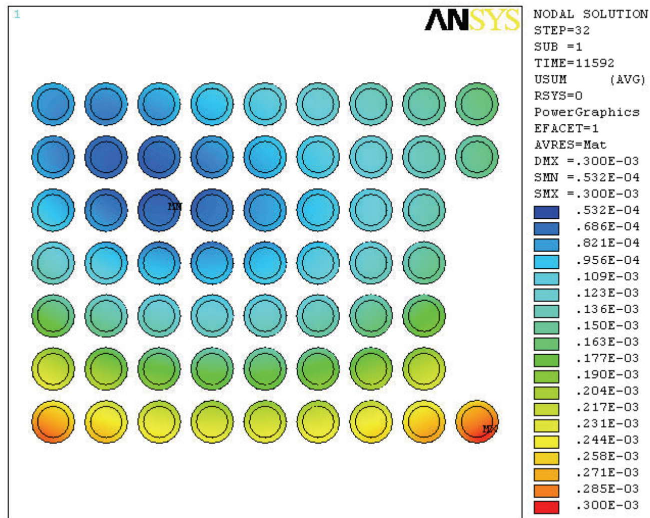

Figure 11: Displacement of the uBall solder-balls at the 32th time step

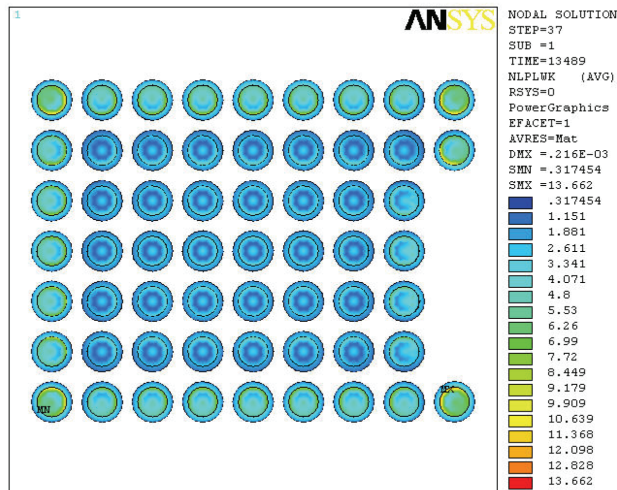

Figure 12: Viscoplastic strain energy density of the uBall solder-balls at the 32th time step

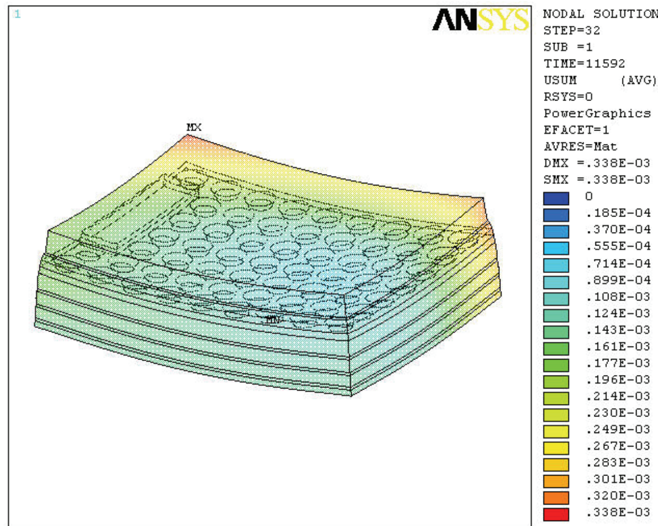

Figure 13: Warping of the uBall WLCSP at the 32th time step (100°C)

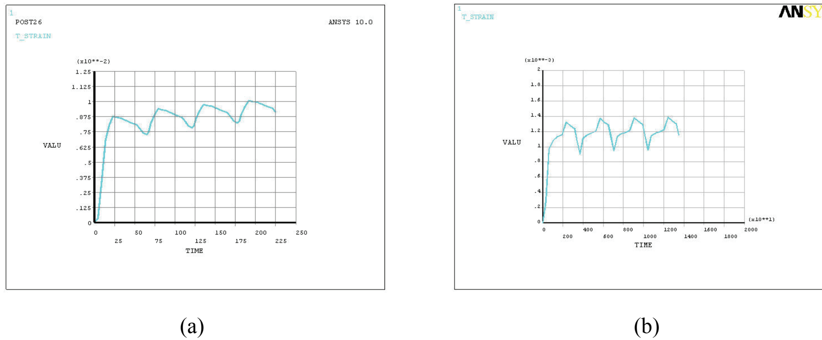

(a) (b)

Figure 14: Variations of the total equivalent strain of (a) STD WLCSP; (b) uBall WLCSP

the yield point, the strain keeps increasing but the stress shows little change. When the number of thermal cycles increases, the accumulated residual strain increases too. This further keeps the stress-strain curve move toward the right hand side. Sequentially, the viscoplastic strain energy density required for calculation of the fatigue life can be extracted from the simulation results. In terms of the reliability of the overall package, the characteristic fatigue life (reliability) of the STD WLCSP for β=2.6 and β=4.0 is 1319 and 1380 thermal cycles, respectively; the reliability of the uBall WLCSP for β=2.6 and β=4.0 is 1902 (cycles) and 1988 (cycles),

respectively.

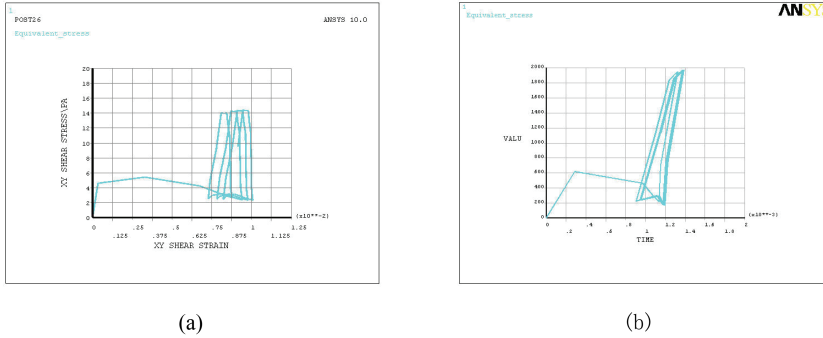

(a) (b)

Figure 15: Stress-strain relation for (a) STD WLCSP; (b) uBall WLCSP

The simulated thermal fatigue lives of the STD and uBall WLCSP samples are summarized in Tab. 4 for comparison with the experimental result.

Table 4: Simulated thermal fatigue lives compared with the experimental result (1315 cycles for STD; 2181 cycles for uBall)

Methodology		Simulated thermal fatigue life (cycles)	Error %
Darveaux's strain-energy based method	STD	1522	+15.74
	uBall	2191	+0.46
Averaged fatigue life (N_{50}, β=2.6)	STD	1319	+0.30
	uBall	1902	-12.84
Averaged fatigue life (N_{50}, β=4)	STD	1380	+4.94
	uBall	1988	-8.85

4 Conclusive remarks

For investigating how underfill may increase the reliability of WLCSP, this paper presents our Finite Element simulations of the thermal fatigue lives of two WLCSP

samples- one standard unit without underfill and the other encapsulated with underfill. Owing to the asymmetrical layout of the package's solder-balls and copper layers, full Finite Element model is required for the analysis, demanding large amounts of elements. To ease the full modeling, the present work proposes a sub-modeling technique, employing a global coarse mesh model in conjunction with a fine mesh model for the vicinity of solder-balls. Additionally, SOLID46 elements were used in ANSYS for modeling the thin layers of PCB to largely reduce the amount of elements. From our numerical simulations and experiments, we draw a conclusion that the use of underfill in WLCSP may increase the reliability by 45%∼65%. In comparison with the experimental results, the numerically simulated values should not be interpreted to be overestimated or underestimated. It is because some manufacturing uncertainties, such as residual stresses, the shape of solder-balls. . . and so forth, may exist even for identical samples. Even the unit's position on PCB may affect the experimental result. This is obvious by checking the experimental result illustrated in Fig. 16 for the thermal fatigue lives of the uBall WLCSP. The thermal fatigue life differs from one to another, where the numbering of units is as in Fig. 4, and we may just give assessment in an average sense. Indeed, the paper provides a expedient yet reliable methodology for assessing the thermal fatigue life of WLCSP.

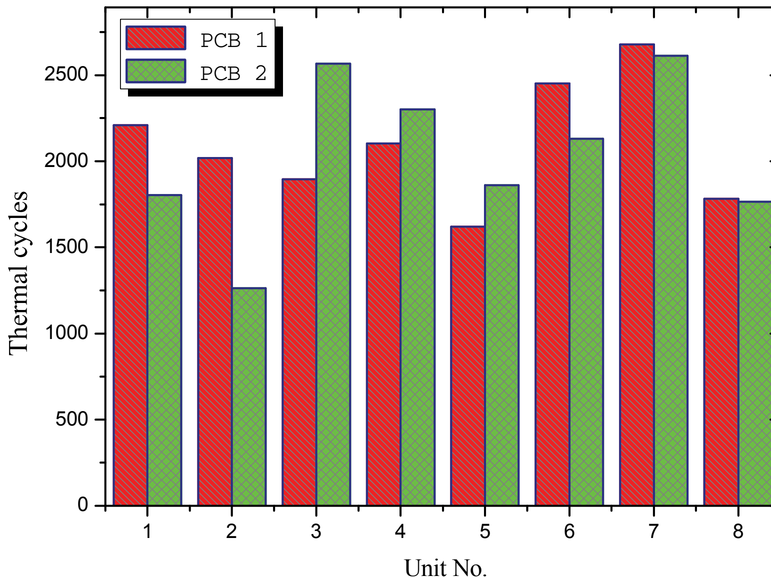

Figure 16: Thermal fatigue lives of uBall WLCSP units

Acknowledgement: The authors would like to express gratitude to National Science Council of Taiwan for the financial support (NSC-96-2221-E-035-011-MY3).

References

Amagai, M. (1999): Chip scale package (CSP) solder joint reliability and modeling, *Microelectronics Reliability*, Vol. 39, Issue 4, pp.463-477.

Anand, L. (1985): Constitutive equations for hot-working of metals. *International Journal of Plasticity*, Vol. 1, pp.213-231.

Cheng, H. C.; Yu, C. Y.; Chen, W. H. (2005): An Effective Thermal-mechanical Modeling Methodology for Large-scale Area Array Typed Packages, *CMES: Computer Modeling in Engineering & Sciences,* Vol. 7, No. 1, pp.1-17.

Chiang, Kuo-Ning; Chou, Chan-Yen; Wu, Chung-Jung; Huang, Chao-Jen; Yew, Ming-Chih (2008): Analytical Solution for Estimation of Temperature-Dependent Material Properties of Metals Using Modified Morse Potential, *CMES: Computer Modeling in Engineering & Sciences,* Vol. 37, No. 1, pp.85-96.

Darveaux, R. (1995): Optimizing the reliability of thin small outline package (TSOP) solder joints, *Advances in Electronic Packaging, ASME*, Vol. 10, No.2, pp.675-685.

Engelmaier, W. W. (1983), Fatigue life of leadless chip carrier solder joints during power cycling, *IEEE Transactions on Components, Hybrids, and Manufacturing Technology*, Vol. 6, pp.232-237.

Knecht, S.; L.R. Fox (1991): Integrated matrix Creep£°Application to accelerated testing and lifetime prediction, *In Solder Joint Reliability£°Theory and Applications*, New York, 1991.

John, L.; Wang, C.P.; John, L.P.; Wataru, N. (1998), *Electronic Packaging: Design, Materials, Process, and Reliability*, McGraw-Hill Companies, Inc.

Lai, Yi-Shao; Wang, Tong Hong; Tsai, Han-Hui; Jen, Ming-Hwa R. (2007): Cyclic bending reliability of wafer-level chip-scale packages, *Microelectronics Reliability,* Vol. 47, Issue 1, pp.111-117.

Lee, W.W.; Nguyen, L.T.; Selvaduray, G.S. (2000)**:** Solder Joint Fatigue Models: Review and Applicability to Chip Scale Packages, *Microelectronics Reliability*, Vol. 40, No. 2, pp.231-244.

Manson, S. S. (1996): Interfaces between Fatigue Creep and fracture, *International Journal of Fracture*, Vol. 2, No.1, pp.327-363.

Pang, J. H. L.; Chong, D. Y. R. (2001): Flip chip on board solder joint reliability analysis using 2-D and 3-D FEA models, *Advanced packaging*, Vol. 24, pp.499-506.

Prabhakar Murthy, D. N.; Bulmer, Michael; Eccleston, John A. (2004): Weibull model selection for reliability modelling, *Reliability Engineering & System Safety,* Vol. 86, Issue 3, pp.257-267.

Sun, F.; Hochstenbach, P.; Van Driel, W.D.; Zhang, G.Q. (2008): Fracture morphology and mechanism of IMC in Low-Ag SAC Solder/UBM (Ni(P)-Au) for WLCSP. *Microelectronics Reliability*, Vol. 48, Issue 8, pp.1167-1170.

Tsai,Tsung-Yueh; Lai, Yi-Shao; Yeh, Chang-Lin, Chen, Rong-Sheng (2008): Structural design optimization for board-level drop reliability of wafer-level chip-scale packages, *Microelectronics Reliability*, Vol. 48, Issue 5, pp757-762.

Weibull, W. (1951): A statistical distribution function of wide applicability, *J. Appl. Mech.-Trans. ASME*, Vol. 18(3), pp.293-297.